ChemComm

Accepted Manuscript

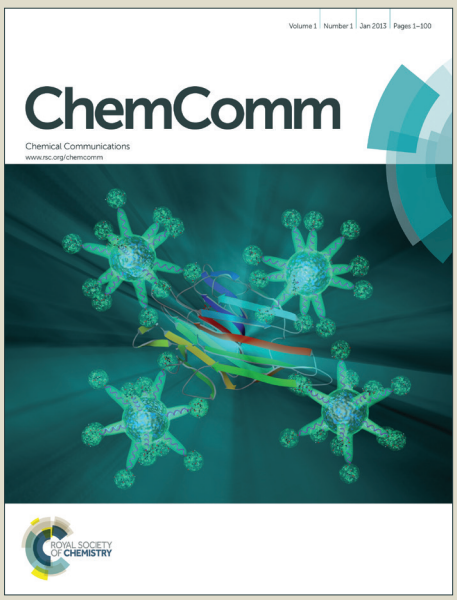

ROYAL SOCIETY OF CHEMISTRY

www.rsc.org/chemcomm

Chemical Communications

COMMUNICATION

Layer-by-Layer Motif Hybridization: Nanoporous Nickel Oxide Flakes Wrapped into Graphene Oxide Sheets toward Enhanced Oxygen Reduction Reaction

Received 00th January 20xx,
Accepted 00th January 20xx

DOI: 10.1039/x0xx00000x

www.rsc.org/

Mohamed B. Zakaria[1,2,3], Victor Malgras*[2], Toshiaki Takei[2], Cuiling Li*[2], and Yusuke Yamauchi*[1,2]

Here we report a novel strategy consisting in hybridizing nanoporous NiO flakes with graphene oxide (GO) sheets. The as-prepared flake-like-shaped nickel cyano-bridged coordination polymers (NiCNNi) are hybridized with GO sheets and thermally treated in air, so the organic materials can be removed without affecting the integrity of the parent GO sheets. Thus, a layer-by-layer construction followed by a thermal treatment can produce a new hybrid nanoporous material consisting of NiO and GO. The obtained hybrid material exhibits an efficient catalytic activity and stability for the oxygen reduction reaction (ORR).

Hybrid materials have many scientific utilities due to the combined effects of two (or more) building blocks. The development of such materials covers a wide range of applications like catalysis, adsorption, electrochemistry, sensor, and energy storage. Therefore, finding efficient methods to prepare these materials in a high yield is of fundamental importance. Among others, a promising concept is the 'layer-by-layer' (LbL) fabrication of nanometer-level layered hybrid structures in a designable manner. LbL approaches are known to be simple, inexpensive, and versatile processes for the fabrication of multilayered hybrid structures with various compositions and have been performed through various interactions, including electrostatic, hydrogen bonding, and charge-transfer, as well as through chemical reactions such as sol-gel, electrochemical coupling, and click reactions.[1] Recently, highly flexible two-dimensional (2D) graphene oxide (GO) sheets have been attracting a lot of attention for their potential in various applications.[2] In particular, the hybridization of GO sheets with various nanomaterials (*e.g.*, nanoparticles) is a promising strategy because of the unique properties arising from the resulting materials.[3]

Fuel cells have attracted a significant interest due to their implementation in highly efficient and clean energy storage systems. Therefore, designing suitable electrocatalysts for oxygen reduction reactions (ORR) is vital in fuel cell research.[4] Tremendous efforts and extensive studies have been done on developing suitable and low-cost catalysts for ORR with high activity. An important challenge, however, remains unsolved. The main problem associated with GO is its intrinsic low ORR activity, which is usually enhanced by either doping with some heteroatoms or hybridization with transition-metal species. Heteroatoms such as nitrogen (N) are generally used to change the charge density in GO and enhance their catalytic activity.[5] On the other hand, transition-metals, such as Ni, Mn, Co, MoO_3, Fe_3O_4, NiO, MoS_2 and WS_2, have recently gained noticeable popularity in various nanocomposite systems owing to their low cost and high activity originating from favourable kinetics phenomenon.[6] Wu *et al.* have reported that Fe_3O_4 nanoparticles supported on 3D nitrogen-doped graphene aerogel are promising for improving the ORR performance.[7]

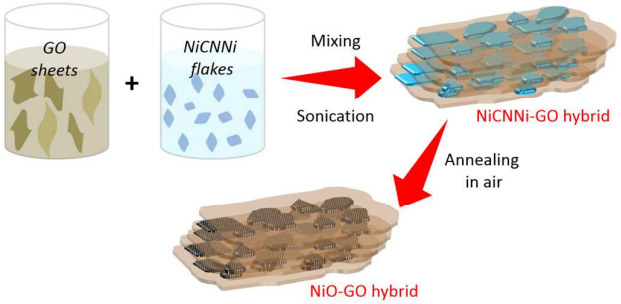

Scheme 1 Schematic presentation of synthesis of NiO-GO hybrid materials by assembling the NiCNNi flakes and GO sheets followed by thermal treatment.

Herein, we propose a new LbL approach for the synthesis of multilayered NiO-GO hybrid materials. Rather disordered interfacial structures in LbL films provide abundant nanospaces, which is advantageous for interlayer molecular diffusion. The electrochemical performance of NiO can be enhanced when combined with GO sheets through proper chemical interaction. The electrochemical analysis performed in this work demonstrates that our NiO-GO hybrid material can serve as an efficient catalyst for

1 *Faculty of Science and Engineering, Waseda University, 3-4-1 Okubo, Shinjuku, Tokyo, 169-8555, Japan.*
E-mails: Malgras.Victor@nims.go.jp; LI.Cuiling@nims.go.jp; Yamauchi.Yusuke@nims.go.jp
2 *World Premier International (WPI) Research Center for Materials Nanoarchitechtonics (MANA), National Institute for Materials Science (NIMS), 1-1 Namiki, Tsukuba, Ibaraki 305-0044, Japan.*
3 *Department of Chemistry, Faculty of Science, Tanta University, Tanta, Gharbeya 31527, Egypt.*

Electronic Supplementary Information (ESI) available: Experimental details and additional characterization data of NiCNNi flakes, NiO flakes, GO sheets,

ORR. It also exhibits a good stability in comparison to PtC-5% catalyst (current loss of about 24.6 % compared to 38.3 %, respectively).

The nickel cyano-bridged coordination polymer (NiCNNi) flakes consist of very thin plates with an average lateral size of around 170 nm (**Fig. S1a**). The flakes are highly crystallized, as confirmed by selected area electron diffraction (SAED) patterns. On the other hand, the GO sheets show a typical 2D morphology with lateral sizes as large as 1 μm (**Fig. S1b**). Their surface is smooth and the sheets are detached from each other. The SAED patterns reveal the typical hexagonal arrangement of a crystalline framework characteristic of GO sheets. The lateral size of the NiCNNi flakes is much smaller than that of GO sheets. The NiCNNi flakes and GO sheets are sonicated separately to form colloidal solutions and their measured zeta potentials are 2.97 mV and -30.7 mV, respectively.[8]

The NiO-GO hybrid materials were synthesized by assembling the NiCNNi flakes and GO sheets followed by thermal treatment (**Scheme 1**). The two colloidal solutions were mixed together under strong sonication. The materials are well dispersed in the suspensions (**Fig. S2**). Through this step, the positively charged NiCNNi flakes become uniformly embedded into the negatively charged GO sheets through electrostatic interactions. By changing the NiCNNi:GO weight ratios, various types of NiO-GO hybrids can be obtained. The zeta potential gradually decreases with increasing the GO content. Scanning electron microscope (SEM) and transmission electron microscopy (TEM) images of the typical NiCNNi-GO hybrids before thermal treatment (NiCNNi:GO =75:25) are shown in **Fig. 1a**. The introduced NiCNNi flakes can clearly be observed inside the GO sheets. During the thermal treatment at 300 °C, the organic group from NiCNNi can be removed to generate nanoporous NiO flakes.[9] Even after calcination, the NiO flakes are still enclosed by the GO sheets. It is worth noticing that the lateral size of NiO flakes remains mostly unchanged after thermal treatment (**Fig. 1b**).

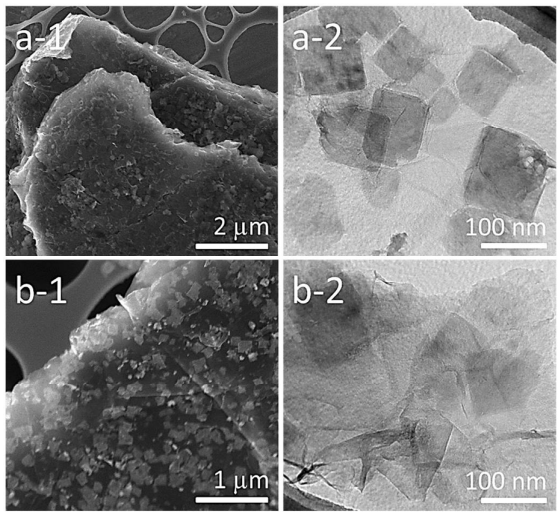

Fig. 1 SEM and TEM images of (a) NiCNNi-GO hybrid (NiCNNi:GO=75:25) before thermal treatment and (b) the corresponding NiO-GO hybrid after thermal treatment.

From the elemental mapping, it is found that carbon, oxygen, and nickel are uniformly distributed over the entire area of the hybrid material (**Fig. S3**). However, it is hard to distinguish the NiO flakes from the GO sheets, because several NiO flakes are overlapped. Cross-sectional TEM images and the corresponding HAADF-STEM and the elemental mapping images show a clear layer-by-layer architecture (**Figs. 2** and **S4**). The introduction of the NiO flakes as spacers prevent restacking or aggregation of the GO sheets.

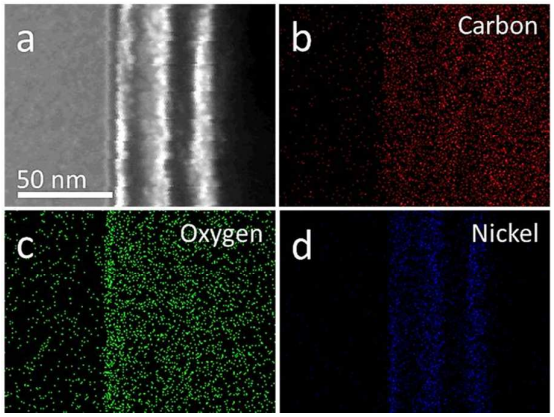

Fig. 2 Cross-sectional HAADF-STEM image and elemental mapping (carbon, oxygen, and nickel) of NiO-GO hybrid prepared from NiCNNi:GO=75:25.

The crystal structure of NiO-GO hybrids after thermal treatment was examined by wide-angle X-ray diffraction (XRD) (**Fig. 3a**). For comparison, the spectra of individually calcined NiO flakes and GO sheets are also displayed. The XRD pattern of NiO-GO hybrids matches with the (111), (200), and (220) crystal planes of a standard NiO crystal structure.[9] Another broad diffraction peak can be assigned to the (002) plane of GO sheets.[10] The Raman spectra of the NiO-GO hybrids and thermally-treated GO sheets are shown in **Fig. 3b**. Along with the characteristic peak of layered graphene oxide at 2913 cm^{-1}, the D and G bands of GO sheets can also clearly be observed.[11] The NiO-GO hybrid shows two additional peaks (at 554 and 1077 cm^{-1}) corresponding to the NiO phase.[12]

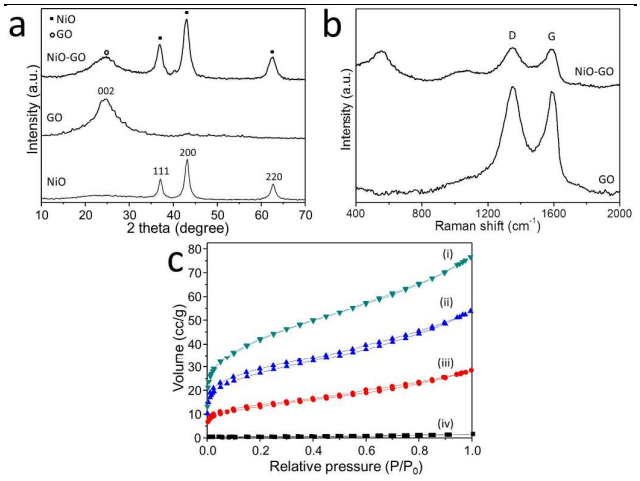

Fig. 3 (a) Wide-angle XRD of the calcined NiO flakes, the calcined GO sheets, and the typical NiO-GO hybrid after thermal treatment, (b) Raman spectra of the calcined GO sheets and the typical NiO-GO hybrid after thermal treatment, (c) N_2 adsorption-desorption isotherms of (i-iii) the NiO-GO hybrids prepared from different NiCNNi:GO compositions [(i) NiCNNi:GO=75:25, (ii) NiCNNi:GO=50:50, (iii) NiCNNi:GO=25:75] and (iv) the calcined GO sheets.

The porosity of the obtained materials was investigated by N_2 adsorption-desorption isotherms (**Fig. 3c**). The corresponding BET surface area is summarized in **Table 1**. The surface area of the hybrid materials appear to increase gradually with increasing the content of NiO flakes in the hybrid system. Actually, the GO sheets possess a relatively small surface area as the layers tend to stack and agglomerate. The introduction of the NiO flakes inside the GO sheets as spacers leads to the enhancement of the overall surface area. From the isotherms, an uptake at low relative pressure ($P/P_0 < 0.1$) can be observed, indicating the presence of micropores. At higher pressure, the adsorption gradually increases without exhibiting any clear capillary condensation step, which is typical of ordered mesoporous materials.[13] It indicates that pore size distribution inside the interlayer space is not uniform.

Table 1. Summary on the surface areas of the obtained samples.

Weight ratios	Surface area ($m^2 g^{-1}$)
NiCNNi:GO = 100:0	78.5
NiCNNi:GO = 75:25	152
NiCNNi:GO = 50:50	99.8
NiCNNi:GO = 25:75	47.8
NiCNNi:GO = 0:100	12.5

The typical NiO-GO hybrid (prepared from NiCNNi:GO=75:25) was examined by X-ray photoelectron spectroscopy (XPS) (**Fig. S5**). The survey spectrum confirms the presence of Ni, O, and C elements in the material. The high resolution spectrum centred on Ni $2p_{3/2}$ reveals that the signal can be divided into at least four contributions, highlighting a multi-coordinated Ni. While the multiplet located at 855.7, 861.0 and 865.3 eV is a typical signature of NiO,[14] the peak at 853.9 eV is believed to originate from the interactions taking place between the NiO flakes and the GO sheets. Indeed, this contribution was not observed for free NiO flakes which are not embedded in GO.[9a] Two peaks at 529.4 eV and 531.4 eV are assignable to the O 1*s* peaks of NiO phase (**Fig. S5c**).[14] The C 1*s* spectrum of GO clearly indicate the presence of a considerable amount of oxidized carbon atoms (**Fig. S5d**). Four types of carbon atoms in different functional groups are observed: non-oxygenated ring (~284.56 eV), C-O (~286.01 eV), C=O (~288.42 eV), and O-C=O (~290.88 eV).[15] It is expected that the NiO flakes are more tightly anchored onto the surface of GO through functional groups containing oxygen.

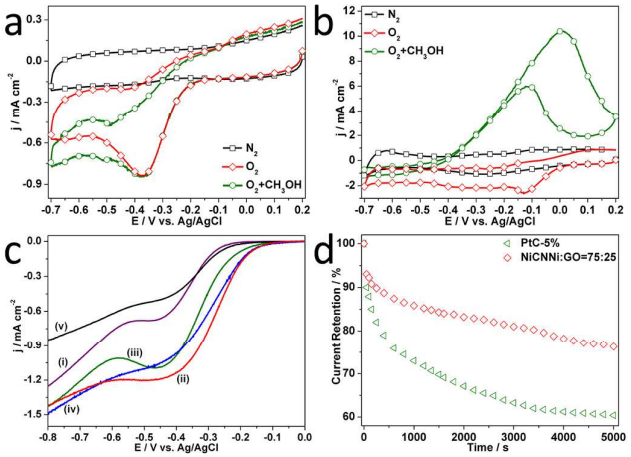

Fig. 4 (a, b) CV curves obtained under N_2- and O_2-saturated 0.1 M KOH, and O_2-saturated 0.1 M KOH together with 0.5 M CH_3OH catalyzed by (a) NiO-GO hybrid prepared from NiCNNi:GO=75:25, and (b) PtC-5%. (c) ORR polarization curves of a RDE modified with (i) the calcined NiO flakes, (ii-iv) the NiO-GO hybrids prepared from different NiCNNi:GO compositions [(ii) NiCNNi:GO=75:25, (iii) NiCNNi:GO=50:50, and (iv) NiCNNi:GO=25:75], and (v) the calcined GO sheets. The plots are obtained in O_2-saturated 0.1 M KOH at a rotation rate of 1600 rpm with a scan rate of 10 mV s^{-1}. (d) Current retention plot during chronoamperometric measurements for NiO-GO hybrid prepared from NiCNNi:GO=75:25 and PtC-5%.

Inspired by the unique structure of our NiO-GO hybrid materials, oxygen reduction reaction (ORR) was selected to examine their performance in energy conversion systems. Cyclic voltammetric (CV) measurements were performed to compare the ORR activity of the hybrid materials prepared from different NiO:GO compositions. The NiO-GO hybrid prepared from NiCNNi:GO=75:25 shows a significant enhancement in ORR activity, compared to the other samples (**Fig. S6**). From the CV curves obtained in O_2-saturated 0.1 M KOH, the NiO-GO hybrid prepared from NiCNNi:GO=75:25 showed an onset potential of about -130 mV (**Fig. 4a**), and a reduction peak at about -370 mV, which are comparable to the previously reported NiO-based catalysts.[16] More importantly, this NiO-GO hybrid shows a good tolerance toward small organic fuels (*e.g.*, methanol), compared to a standard 5% Pt supported on carbon (abbreviated as PtC-5%) (**Fig. 4a-b**).[17] All the results indicated that our NiO-GO hybrid materials are good candidates for ORR and do not suffer from the cross over effects of organic fuels.

The ORR performance was further tested by using a rotating disk electrode (RDE) in an O_2-saturated 0.1 M KOH solution at a rotation speed of 1600 rpm. The linear sweep voltammograms (LSVs) of all the samples are shown in **Fig. 4c**. The electrochemical behavior toward the ORR varies depending on the NiO:GO compositions. The NiO-GO hybrid prepared from NiCNNi:GO=75:25 shows the best performance from the standpoints of both onset potential and limiting current. The onset potential of NiO-GO hybrid prepared from NiCNNi:GO=75:25 (-100 mV) for the ORR is more positive (-100 mV) compared to the other samples [NiO (-180 mV), NiO-GO hybrid prepared from NiCNNi:GO=50:50 (-100 mV), NiO-GO hybrid prepared from NiCNNi:GO=25:75 (-140 mV), and GO (-120 mV)]. A larger surface area can be obtained by increasing the proportion of NiO flakes. The NiO-GO hybrid with high surface area probably tends to decrease the mass transport resistance and facilitate the access of the electrolyte to the active sites, which is greatly beneficial during the ORR process.[18] A chronoamperometric measurement over a time period of 5000 s was further performed on the NiO-GO hybrid, and benchmarked to the PtC-5% catalyst. The current retention performance is shown in **Fig. 4d**. The NiO-GO hybrid shows a current loss of 24.6 %, which is much less than for the PtC-5% catalyst (38.3 %).

In conclusion, we successfully prepared NiO-GO hybrid materials with high surface area through the thermal conversion of NiCNNi-GO hybrids. The NiO flakes are uniformly distributed and tightly anchored onto the surface of the GO sheets, thereby forming a robust hetero-layered structure assembled through LbL process. The NiO-GO hybrids exhibit an efficient catalytic activity for ORR. Combining the desirable electrochemical properties of both NiO and GO lead to a synergetic improvement of their electrocatalytic activity. Our strategy can be applicable in the future for the preparation of various functional metal oxides wrapped in GO sheets for promising electrocatalytic applications.

References

1 (a) G. Decher, J. D. Hong and J. Schmitt, *Thin Solid Films*, 1992, **210-211**, 831, (b) S. S. Shiratori and M. F. Rubner, *Macromolecules*, 2000,

33, 4213, (c) N. Cini, T. Tulun, G. Decher and V. Ball, *J. Am. Chem. Soc.*, 2010, **132**, 8264, (d) J. Choi, R. Suntivich, F. A. Plamper, C. V. Synatschke, A. H. E. Müller and V. V. Tsukruk, *J. Am. Chem. Soc.,* 2011, **133**, 9592, (e) K. Ariga, Y. Yamauchi, G. Rydzek, Q. Ji, Y. Yonamine, K. C.-W. Wu and J. P. Hill, *Chem. Lett.,* 2014, **43**, 36.

2 (a) R. R. Salunkhe, S.-H. Hsu, K. C.-W. Wu and Y. Yamauchi, *ChemSusChem*, 2014, **7**, 1551, (b) Y. Su, S. Li, D. Wu, F. Zhang, H. Liang, P. Gao, C. Cheng and X. Feng, *ACS Nano*, 2012, **6**, 8349, (c) X. Meng, D. Geng, J. Liu, M. N. Banis, Y. Zhang, R. Li and X. Sun, *J. Phys. Chem. C*, 2010, **114**, 18330, (d) G. Williams, B. Seger and P. V. Kamat, *ACS Nano*, 2008, **2**, 1487.

3 (a) X. Zhou, X. Huang, X. Qi, S. Wu, C. Xue, F. Y. C. Boey, Q. Yan, P. Chen and H. Zhang, *J. Phys. Chem. C*, 2009, **113**, 10842, (b) Z. Zhang, F. Xu, W. Yang, M. Guo, X. Wang, B. Zhang and J. Tang, *Chem. Commun.,* 2011, **47**, 6440, (c) S. Yang, G. Cui, S. Pang, Q. Cao, U. Kolb, X. Feng, J. Maier, K. Mllen, *ChemSusChem*, 2010, **3**, 236.

4 Y. Agawa, H. Tanaka, S. Torisu, S. Endo, A. Tsujimoto, N. Gonohe, V. Malgras, A. Aldalbahi, S. M. Alshehri, Y. Kamachi, C. Li and Yusuke Yamauchi, *Sci. Technol. Adv. Mater*, 2015, **16**, 024804.

5 (a) A. Aijaz, N. Fujiwara and Q. Xu, *J. Am. Chem. Soc.,* 2014, **136**, 6790, b) L. Lin, Q. Zhu and A. W. Xu, *J. Am. Chem. Soc.,* 2014, **136**, 11027, (c) Y. Meng, D. Voiry, A. Goswami, X. Zou, X. Huang, M. Chhowalla, Z. Liu and T. Asefa, *J. Am. Chem. Soc.*, 2014, **136**, 13554.

6 (a) T. Y. Ma, S. Dai, M. Jaroniec and S. Z. Qiao, *J. Am. Chem. Soc.,* 2014, **136**, 13925, (b) R. Wu, D. P. Wang, X. Rui, B. Liu, K. Zhou, A. W. K. Law, Q. Yan, J. Wei and Z. Chen, *Adv. Mater.,* 2015, **27**, 3038, (c) N. Jiang, B. You, M. Sheng and Y. Sun, *Angew. Chem. Int. Ed.,* 2015, **54**, 6251, (d) Y. Shi, J. Wang, C. Wang, T. T. Zhai, W. J. Bao, J. J. Xu, X. H. Xia and H. Y. Chen, *J. Am. Chem. Soc.,* 2015, **137**, 7365.

7 Z. S. Wu, S. Yang, Y. Sun, K. Parvez, X. Feng and K. Müllen, *J. Am. Chem. Soc.,* 2012, **134**, 9082.

8 (a) W. Zhu, K. Liu, X. Sun, X. Wang, Y. Li, L. Cheng and Z. Liu, *ACS Appl. Mater. Interfaces*, 2015, **7**, 11575, (b) S. Yang, X. Feng, S. Ivanovici and K. Müllen, *Angew. Chem. Int. Ed.,* 2010, **49**, 8408, (c) L. Zhang, J. Xia, Q. Zhao, L. Liu and Z. Zhang, *Small,* 2010, **6**, 537.

9 (a) M. B. Zakaria, M. Hu, R. R. Salunkhe, M. Pramanik, K. Takai, V. Malgras, S. Choi, S. X. Dou, J. H. Kim, M. Imura, S. Ishihara and Y. Yamauchi, *Chem.-Eur. J.*, 2015, **21**, 3605, (b) M. Hu, S. Ishihara and Y. Yamauchi, *Angew. Chem. Int. Ed.,* 2013, **52**, 1235.

10 (a) J. Shen, Y. Hu, M. Shi, X. Lu, C. Qin, C. Li and M. Ye, *Chem. Mater.*, 2009, **21**, 3514, (b) S. Park, J. An, J. R. Potts, A. Velamakanni, S. Murali and R. S. Ruoff, *Carbon*, 2011, **49**, 3019.

11 N. L. Torad, R. R. Salunkhe, Y. Li, H. Hamoudi, M. Imura, Y. Sakka, C. C. Hu and Y. Yamauchi, *Chem.-Eur. J.,* 2014, **20**, 7895.

12 (a) B. Zhao, J. Song, P. Liu, W. Xu, T. Fang, Z. Jiao, H. Zhang and Y. Jiang, *J. Mater. Chem.,* 2011, **21**, 18792, (b) N. Mironova-Ulmane, A. Kuzmin, I. Steins, J. Grabis, I. Sildos and M. Pärs, *J. Phys: Conference Series,* 2007, **93**, 012039, (c) W. Wang, Y. Liu, C. Xu, C. Zheng and G. Wang, *Chem. Phys. Lett.,* 2002, **362**, 119.

13 (a) K. Ariga, A. Vinu, Y. Yamauchi, Q. Ji and J. P. Hill, *Bull. Chem. Soc. Jpn.,* 2012, **85**, 1, (b) V. Malgras, Q. Ji, Y. Kamachi, T. Mori, F. Shieh, K. C. W. Wu, K. Ariga and Y. Yamauchi, *Bull. Chem. Soc. Jpn.*, 2015, **88**, 1171.

14 (a) X.-Q. Li and W.-X. Zhang, *Langmuir*, 2006, **22**, 4638, (b) M. C. Biesinger, B. P. Payne, A. P. Grosvenor, L. W. M. Lau, A. R. Gerson and R. St. C. Smart, *Appl. Sur. Sci.,* 2011, **257**, 2717, (c) A. P. Grosvenor, M. C. Biesinger, R. St. C. Smart and N. S. McIntyre, *Surf. Sci.,* 2006, **600**, 1771, (d) M. H. Koppelman and J. G. Dillard, *Clay. Clay Miner.,* 1977, **25**, 457.

15 (a) S. Pei and H.-M. Cheng, *Carbon*, 2012, **50**, 3210, (b) D. Yang, A. Velamakanni, G. Bozoklu, S. Park, M. Stoller, R. D. Piner, S. Stankovich, I. Jung, D. A. Field, C. A. Ventrice Jr and R. S. Ruoff, *Carbon*, 2009, **47**, 145, (c) D. R. Dreyer, S. Park, C. W. Bielawski and R. S. Ruoff, *Chem. Soc. Rev.,* 2010, **39**, 228.

16 (a) M. Srivastava, M. E. Uddin, J. Singh, N. H. Kim and J. H. Lee, *J. Alloy. Compd.*, 2014, **590**, 266. (b) Q. Wu, L. Jiang, Q. Tang, J. Liu, S. Wang and G. Sun, *Electrochim. Acta*, 2013, **91**, 314.

17 (a) Y. Xiao, C. Hu, L. Qu, C. Hu and M. Cao, *Chem.-Eur. J.*, 2013, **19**, 14271, (b) J. Cruickshank and K. Scott, *J. Power Sources*, 1998, **70**, 40, (c) C. Y. Du, T. S. Zhao and W. W. Yang, *Electrochim. Acta*, 2007, **52**, 5266.

18 (a) C. Li, T. Sato and Y. Yamauchi, *Angew. Chem. Int. Ed.*, 2013, **52**, 8050, (b) J. Tang, J. Liu, C. Li, Y. Li, M. O. Tade, S. Dai, Y. Yamauchi, *Angew. Chem. Int. Ed.,* 2015, **54**, 588.